Soft Matter

ROYAL SOCIETY OF CHEMISTRY

PAPER

View Article Online
View Journal | View Issue

Cite this: *Soft Matter*, 2020, **16**, 8612

Rising obstacle in a one-layer granular bed induced by continuous vibrations: two dynamical regimes governed by vibration velocity

Hui Zee Then, Teruyo Sekiguchi and Ko Okumura *

Received 1st June 2020,
Accepted 29th July 2020

DOI: 10.1039/d0sm01021a

rsc.li/soft-matter-journal

The rising motion of an obstacle in a vibrated granular medium is a classic problem of granular segregation, and called the Brazil nut (BN) effect. Identification of the controlling vibration parameters of the effect is a long-standing problem. The simple possibility that the BN effect can be characterized solely by vibration velocity has recently been pointed out. The issue has become controversial over the long history of research, with only a few systems providing evidence for this simple possibility. Here, we investigate the rising motion of an obstacle in a vertically positioned one-layer granular bed under continuous vibrations. We find the rising motion is composed of two distinct regimes, and the first and second regimes are both governed, in terms of vibration parameters, solely by the vibration velocity. We further demonstrate simple scaling laws that well describe the two regimes. Our results support the emergent simple possibility for the controlling parameters of the BN effect and suggest that this feature could be universal. We propose two possible mechanisms of convection and arch effect for the two distinct regimes and demonstrate that these mechanisms explain the scaling laws followed by our experimental data.

I. Introduction

When a cell that contains a mixture of grains of large and small sizes is vibrated, the large grains tend to rise up in the cell. This effect is a typical example of size segregation of grains by shaking, known as the Brazil nut (BN) effect.[1,2] With pioneering work using simulations[3] and experiments,[4–6] many studies have been performed in the field of physics to explain the effect. As a result a number of physical mechanisms of the phenomenon have been proposed, which include void filling,[7] convection,[5] and the arching effect.[6]

However, as for the controlling vibration parameters of the BN effects, our understanding has become controversial. It was believed that characterization of the convection-driven rising motion requires at least two vibration parameters: the acceleration and frequency.[8,9] However, several years ago, it was clearly shown that the convection-driven rising motion is characterized, in terms of vibration parameters, solely by the vibration velocity, in a wide range of experimental parameters.[10] Subsequently, a detailed study on the granular convection induced by vibration revealed that the convection velocity is well characterized by the vibration velocity,[11] supporting the recent study.[10] However, despite a long history of research, the vibration-velocity governed BN effect has been reported only in a few cases,[10,12] and the problem of the controlling vibration parameters has become controversial (*e.g.*, well-known MRI studies[8,13] did not demonstrate that their data can be characterized solely by vibration velocity). Therefore, providing experimental data that can be characterized solely by vibration velocity in different systems is an emergent important issue for settling this long-standing issue.

In order to elucidate the controlling vibration parameters in the BN effect, we investigate the rising motion in a one-layer granular bed under continuous vibration. As a result, we find that the dynamics are divided into first and second regimes, and both are well characterized solely by the vibration velocity through simple scaling laws. In addition, we propose possible mechanisms of convection and arch effect for the two regimes, and demonstrate that these mechanisms explain the scaling laws followed by the experimental data.

II. Experiment

The setup is shown in Fig. 1a. A cell of thickness 1.2 mm was filled with beads of average diameter 1.0 mm and a stainless-steel disk of thickness 1.0 mm. The cell is mounted on a vibration system, which causes a rising motion of the disk in a granular medium (consisting of one layer of beads) with the disk sliding freely on its circumference in the medium.

Physics Department and Soft Matter Center, Ochanomizu University, Tokyo 112-8610, Japan. E-mail: okumura@phys.ocha.ac.jp

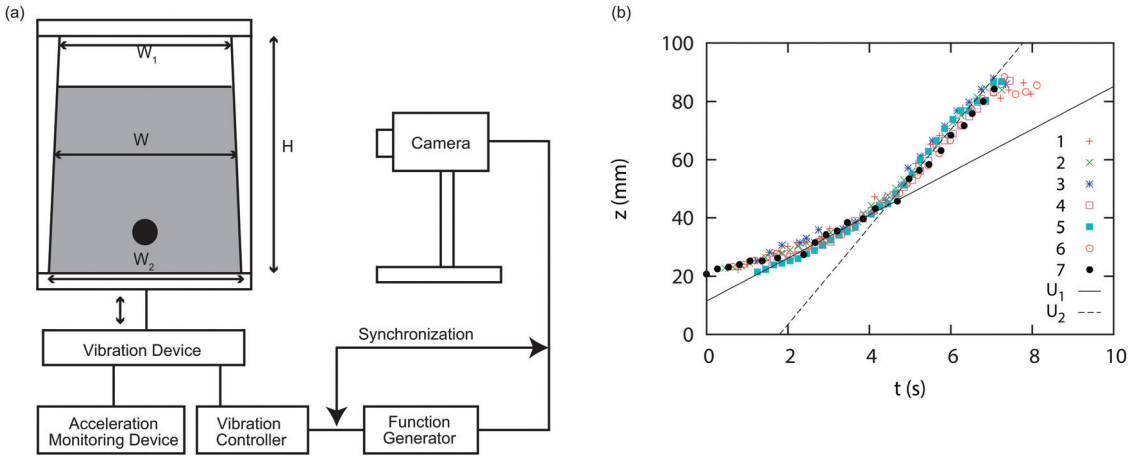

Fig. 1 (a) Experimental setup. The bottom of the vertically-positioned cell is set as the origin of the vertical axis z. (b) The position z of the intruder (D = 12 mm) as a function of time t for a cell (W = 85 mm) at the vibration frequency f = 30 Hz and the vibration acceleration a = 50 m s^{-2}. The ascent of the intruder proceeds in two stages. The slopes indicated by the solid and dashed lines respectively show the corresponding two velocities U_1 and U_2. See the text for details.

We used a cell with side walls slightly down-facing with an angle of about 5° (specified below) throughout this study. A slight side-wall angle was necessary to observe stable rising motion of the disk. When the side walls were vertical, the rising motion was less smooth and less reproducible. Dependence on the angle may originate from a weak friction on the side walls (their surfaces are smooth) and a relatively weak polydispersity of our beads (the bead diameters were approximately in the range 0.9–1.15 mm), which tends to create lattice structures. With a slight down-facing angle, lattice structures tend to be broken and the movement of beads near the side walls are restrained as in the case when friction on the side wall is strong. Note that the importance of friction on the vertical side wall for convection has been pointed out, and it has also been demonstrated that the introduction of an angle in the opposite up-facing direction can reverse the direction of convection.[5] However, in the present case, the angle was smaller and introduced to conduct a reproducible study of the BN effect. In this sense, the slight side-wall angle contributes to enhance the effect of polydispersity and friction near the side walls.

A cell of thickness t = 1.2 mm was made from two transparent acrylic plates of thickness 3 mm, separated with spacers of thickness t. The cell height H was fixed to 140 mm. The top and bottom widths of the cell, W_1 and W_2 (see Fig. 1a), were slightly different with a finite angle α defined by $\tan\alpha = (W_2 - W_1)/(2H)$. The width of the cell W was defined as $W = (W_1 + W_2)/2$ for convenience. The cell width W was either 55, 80, 85, or 105 mm. In the case of W = 85 mm, W_1 and W_2 were set to W_1 = 80 and W_2 = 90 mm, while W_1 and W_2 for different W were determined such that the angle α was the same with that for W = 85 mm, *i.e.*, α was fixed to a value $\alpha = \arctan[(90-80)/(2 \times 140)]$ ($\sim 5°$).

The cell contained a metal disk (diameter D = 12, 15, or 18 mm, with thickness 1 mm), which plays the role of an obstacle or an intruder, and one layer of small balls of aluminum oxide with average diameter d = 1 mm (AL-9, AS ONE Corp.), which play the role of grains or a granular medium. The balls filled the cell with the obstacle to a depth H_0 = 100 mm (or 80 nm in a few cases). The density of disks (7.7–7.9 g cm^{-3}) are larger than that of the small alumina balls (3.95 g cm^{-3}).

The cell containing the obstacle and grains was mounted vertically on a vibration generator system (m060/MA1-CE, IMV Corp.), which was controlled by a multi-function generator (WF1948, NF Corp.) and monitored by an acceleration meter (VM-1970, IMV Corp.). Digital images were obtained with a CCD camera (STC-MB33USB, SENTECH Co., Ltd), which was synchronized with the vibration system through the function generator.

The vibration generation system can produce continuous sinusoidal waves with control of the angular frequency ω and amplitude A. The sinusoidal wave can be characterized by the vibration velocity $v = \omega A$, acceleration $a = \omega^2 A$, and frequency $f = \omega/(2\pi)$.

III. Results

A. Rising motion

As shown in Fig. 1b, the intruder rises in the layer of grains with time under vibration. The different symbols in the graph correspond to different ascent experiments performed under the same conditions specified in the caption. As seen in the plot, all the data points collapse onto a master curve except near the starting point, demonstrating a reasonable reproducibility of the experiment. The master curve can be divided into two regimes, characterized by two velocities U_1 and U_2, as indicated in the plot. The linearity in the second region was more visible than in the first. The determination of the slopes corresponding to U_1 and U_2 is explained below in detail. The crossover depth was around 40 to 60 mm in our parameter ranges, but it was not sensitive to parameter changes (it was difficult to find a systematic trend). The initial position was set to z = 20 mm. When the intruder was initially placed at a deeper

position, the rising motion of the disk became less reproducible near the bottom. A critical initial depth for rising was difficult to define because it seemed to be dependent on uncontrollable initial configurations of the beads.

B. Simple scaling laws for U_1 and U_2

Fig. 2a and b, which show the two velocities U_1 and U_2, respectively, obtained under various conditions as a function of the vibration acceleration a, suggest that these velocities are not governed solely by the vibration acceleration. In contrast, as demonstrated in Fig. 2c and d, the two velocities are controlled solely by the vibration velocity: after carefully looking at the dependence of the data on experimental parameters, we found that the data can be well described by the relations

$$\frac{U_1}{\sqrt{gd}} = k_1 \frac{v^2}{Wg} \quad (1)$$

$$\frac{U_2}{v_c} = k_2 \frac{D(v - v_c)}{Wv_c} \quad (2)$$

where g is the gravitational acceleration with $v_c = 126 \pm 5$ mm s^{-1}, $k_1 = 0.88 \pm 0.022$ and $k_2 = 0.85 \pm 0.016$. The fitting parameter v_c was introduced because in the U_1 *vs.* v plot the data were on a straight line and the line intersects with the v axis at the same point (within experimental errors), irrespective of D and W. Note v_c is of the order of $\sqrt{gd}$, which is a natural velocity scale in the present problem, as appears in eqn (1).

The following information could be gleaned from the values of k_1 and k_2. (I) The fact that k_1 and k_2 are both close to one confirms that the orders of magnitude predicted by eqn (1) and (2) are consistent with our experimental data. (II) The fact that the standard deviations for k_1 and k_2 thus obtained are only a few per cent (they are 2.51 and 1.85%, respectively) suggests that our experimental data and analyses are of high quality.

Details for obtaining the values and error bars for Fig. 2c and d are explained as follows. We prepared n sets of data under the same experimental conditions, *i.e.*, for a set of (D,W,f,v). For each set of data, we first determined the second region exploiting its clear linearity with a slope (corresponding to U_2), and the data in the remaining region was fit by a straight line with another slope (corresponding to U_1). This second fit was conducted by selecting a linear region as wide as possible with the criterion that *the coefficient of determination* became below 0.98 (this coefficient was determined by $1 - \sum_{i=1}^{m} (z_i - z_P)^2 \Big/ \sum_{i=1}^{m} (z_i - z_A)^2$ where z_P and z_A are the predicted and average values, respectively, for m data of z_i). This well-defined method to determine U_1 was used based on the following observations. (1) Rising motion was unstable near the starting point with less reproducibility. (2) However, before the second region, which is clearly linear, another linear region tended to appear and its slope was reproducible although its width was not. These features are visible in Fig. 1b if we compare the slopes and the experimental data. Note that k_1 and k_2 used in Fig. 1b are the same values obtained from Fig. 2c and d. In this way, we obtained n different sets of (U_1, U_2) for a single set of (D,W,f,v). If n was larger than 10 we employed the standard deviation as the error bar. Otherwise, the highest and lowest positions of the error bar were determined by the

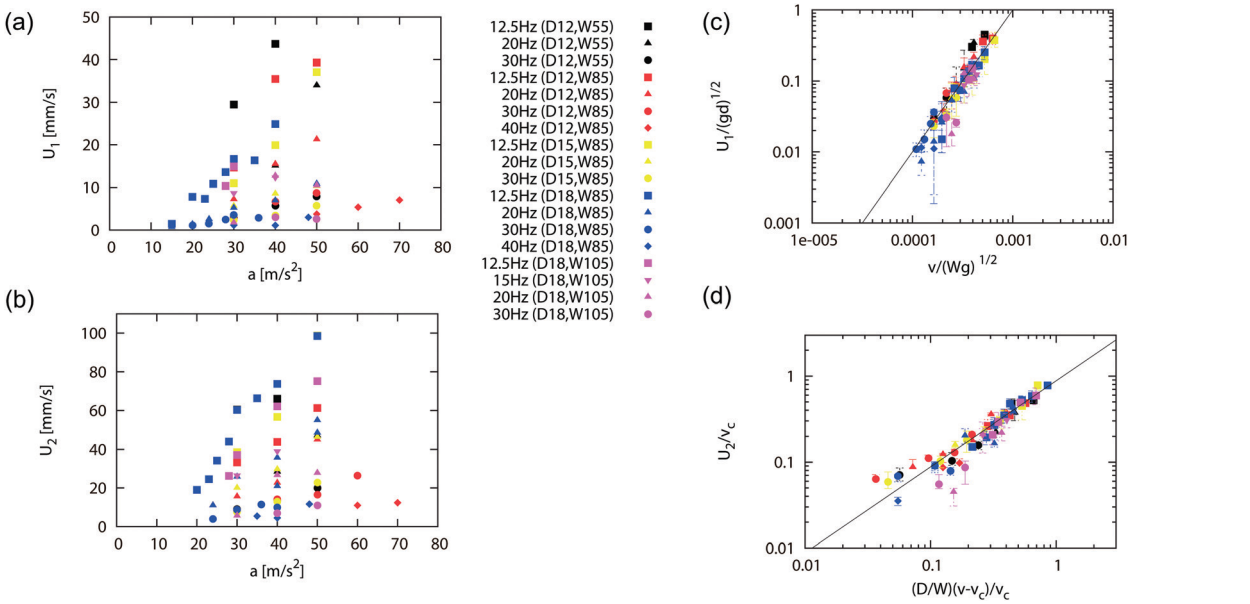

Fig. 2 (a and b) The rising velocity in the first regime U_1 and that in the second regime U_2 as a function of the vibration acceleration a for different vibration frequencies, 12.5 Hz (squares), 20 Hz (triangles), 30 Hz (circles) and 40 Hz (diamonds). Data for (D,W) = (12,55), (12,85), (15,85), (18,85) and (18,105) are represented by black, red, yellow, blue, and magenta symbols, respectively. (c) All the data in (a) replotted with renormalized axes. The line with slope 2 represents eqn (1) with $k_1 = 0.88 \pm 0.022$. (d) All the data in (b) replotted with renormalized axes. The line with slope 1 represents eqn (2) with $k_2 = 0.85 \pm 0.016$.

maximum and minimum values, respectively. Some data in Fig. 2 and the data in Fig. 1b were obtained at H_0 = 80 mm but the U_1 and U_2 obtained at H_0 = 100 and 80 mm were indistinguishable, as demonstrated by a good agreement between the data and the solid and dashed lines in Fig. 1b.

IV. Physical interpretations

A. First regime: ascent by filling the created arch-shaped void

The physical mechanism for the rise in the first regime can be considered as a result of the small beads filling an arch-shaped void created at the bottom of the cell during vibration, as illustrated in Fig. 3a. These arch shapes are created as a result of time-sequential motion as shown in Fig. 3b.

For simplicity, we consider the case $a \gg g$ to gain physical insight into this sequential motion (in fact, the ascent can be observed only when $a > g$, as also reported in ref. 10 and 14). When a sinusoidal wave is applied to the system, the normal force acting on the system (total mass M) of one grain layer and the intruder from the cell bottom is given by $N = -Mg - M\alpha$, as long as the system holds contact with the cell bottom, if we neglect the friction effect near the side walls. Here, $\alpha = -a\cos\omega t$ is the acceleration corresponding to the movement of the position of the base plate of the cell described by $z = A\cos\omega t$. This means, if $a \gg g$, at the moment when the cell moves upwards from the central position of vibration, $z = 0$, the normal force N becomes zero and the system starts a parabolic motion under gravity with the initial speed comparable to $v = \omega A$. The maximum height of the parabolic motion scales as h with $v^2 \simeq gh$ (this relation is exact in Newtonian mechanics, in the absence of side walls with the constraint that all the particles are on the vertical plane; thus the relation tends to hold in the central region if the wall distance is large and friction with the front and back walls is small, as in the present case). Furthermore, if the maximum height h is considerably larger than the vibration amplitude A (this implies ω is large in the light of the relation $a = \omega^2 A$), the maximum height of the layer bottom relative to the cell bottom is comparable to h, which is the same under a fixed v. In summary, the maximum height tends to scale as $h \simeq v^2/g$.

However, small beads close to the side walls cannot move (relative to the cell) because of the friction effect near the side walls, while small beads around the center of the cell repeatedly go up with the intruder under vibration till the maximum height comparable to $h \simeq v^2/g$ (relative to the cell bottom) as estimated above. This leads to the formation of a velocity gradient in the granular layer in the direction of cell width, which results in an arch-shaped void at the bottom of the layer as shown by the snapshots in Fig. 3b. During the formation of an arch-shaped void, some beads close to the bottom of the layer enter into the void due to the velocity gradient, which results in a shear force. As a result, the height of the intruder relative to the cell bottom when it is next pushed to the cell bottom becomes higher than before. This is the mechanism of ascent by void filling.

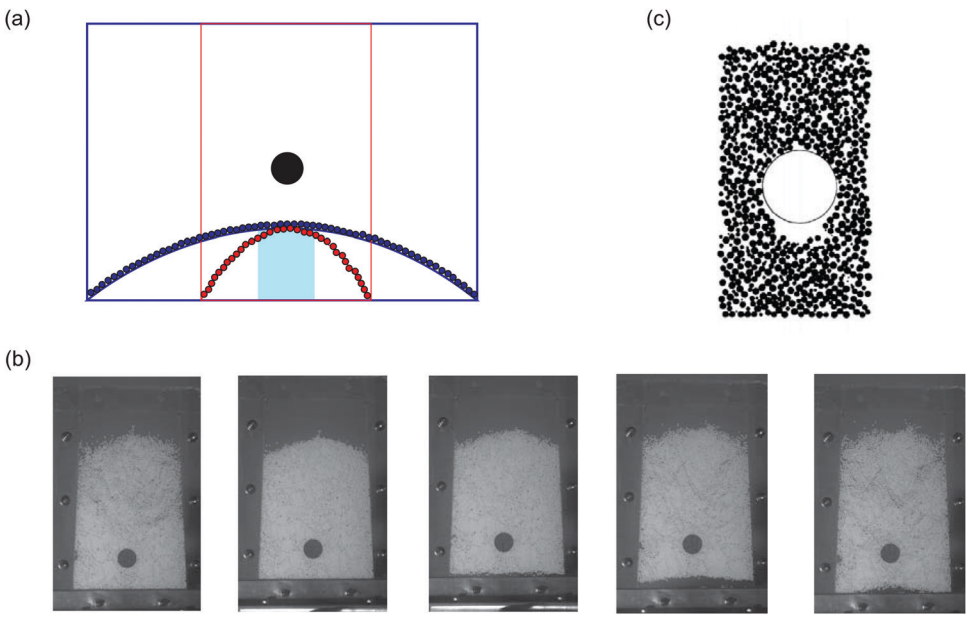

Fig. 3 (a) Illustration of two arches repeatedly formed at the bottom of a layer during vibration. The width of the arch is determined by the distance between the side walls of the cell. This illustration superimposes two cases, a wider cell and a narrower cell at the same vibration velocity when the arch becomes most significant (such a moment, corresponding to the second rightmost snapshot in Fig. 3b below, repeatedly appears with a given frequency). The height at the center is the same for the two cells because it is set by v^2/g as explained in the text. (b) Sequential snapshots, separated by 10 ms, of a cell of W = 85 mm under vibration at f = 12.5 Hz and a = 30 mm s^{-2} with an intruder of D = 15 mm. The arch-shaped void is created at the bottom of the granular layer, which is most visible in the photograph second from the right. (c) Void filling mechanism suggested in previous studies: black particles continuously fill up the void created beneath the intruder during shaking, which results in the rise of the intruder. Figure (c) is reproduced with permission from ref. 7, Copyright, American Physical Society, 1992.

This mechanism of the ascent by void filling is consistent with the dependence of the ascent velocity U_1 on the cell width W and on the vibration velocity v, predicted in eqn (1). As long as $a \gg g$, for a fixed v, the maximum height of the arch tends to be the same (comparable to h given above), meaning that the velocity gradient increases as W decreases. Accordingly, we expect that U_1 increases as W decreases, which qualitatively explains why U_1 scales with $1/W$ in eqn (1). For a fixed W, since h tends to scale with v^2, if the void were completely filled, U_1 would scale with ωv^2 by noting that the period of vibration scales as $1/\omega$. However, the void filling is much less effective, as observed in Fig. 3b, because the filling is induced by a shear force and thus takes a finite time. This implies the effectiveness of void filling increases with the period $\simeq 1/\omega$. Thus, expect the ascent per vibration may scale not with ωv^2 but this factor multiplied with the effectiveness factor $1/\omega$, which results in U_1 scaling with v^2, in accordance with eqn (1). Note that the number of beads falling off from the arch into the void will increase as the life time of the transient arch increases, *i.e.*, the period of vibration increases (as shear tends to increase the number). In this sense, the effectiveness of void filling increases with $1/\omega$ (as W decreases the effectiveness reducing shear).

According to eqn (1), U_1 is independent of the disk diameter D. This is in contrast with the ascent ascribed to the void filling mechanism in previous studies.[2,3,7] The void considered in previous studies is not the arch-shaped void but a void formed beneath the disk as illustrated in Fig. 3b. This implies the ascent velocity increases with D. However, in the present case, the size of the arch-shaped void is independent of the size of the disk (this is because the width is set by W and the height is set by v^2/g as explained above), and, thus, it is natural that U_1 is independent of D.

B. Second regime: ascent by convection

The physical mechanism for the rise in the second regime can be considered as a result of convection. To draw this conclusion, we put a steel bead (silver color) of the same diameter (1 mm) in a layer of alumina beads (white color) and track the movement of the steal bead (density 7.85 g cm^{-3}). As seen in a typical result shown in Fig. 4a, a convective roll motion is observed in the right side of the cell. By analyzing the chronological order of black dots corresponding to the steal bead, it is revealed that the flow is upward in the center of the cell and is downward near the wall. From symmetry, a similar roll should exist in the left side of the cell. The upward flow near the center starts at a certain height where two rolling flows merge, one from the right side and the other from the left side, and this height seems to correspond to the height of the transition from the first regime characterized by U_1 to the second by U_2. Accordingly, we can expect that the rising motion in the second regime is due to the convective roll motion.

For later discussion, we here confirm experimentally that the width of the downward flow developed near a side wall is comparable to the size of the grain, which is consistent with previous reports.[5] This is shown in Fig. 4b quantifying the width of the downward flow near the wall. To obtain this plot, we took snapshots of a vibrated cell with a single tracer particle and superposed only a selected set of snapshots for a given duration, where we selected only the snapshots in which the particle moved down compared with its previous snapshot. An example of such superimposed snapshots is given in Fig. 4c. We estimated the width from the maximum width (as a function of height) as indicated in the figure. The width thus obtained is given as a function of time for two cells with different width as in Fig. 4b. As shown in the plot, the width saturates with time and the saturated value, which is several times the grain size, is independent of the cell width.

The independence of the width of the downward flow near the side wall from the cell width, confirmed in Fig. 4b is physically natural because such a downward flow is caused by the friction effect near the side walls, and this effect should be the same for cells of different width as long as the side walls are well separated compared with the width of the downward flow. In addition, this implies that the flux of the downward flow is independent from the cell width W for a given v, and that the shear force which governs the flow is characterized not by v/W but by v/d.

Considering that the flow flux is conserved in the rolling motion, we expect that upwards velocity in the absence of the

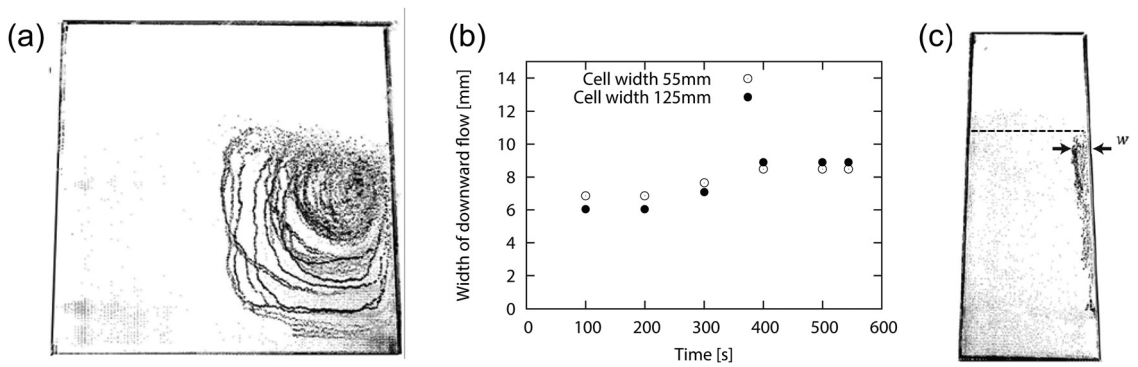

Fig. 4 (a) Convection roll visualized by superposition of snapshots obtained under the existence of a single tracer particle in the cell. Images were obtained at frequency f = 12.5 Hz and acceleration a = 50 m s^{-2} with a cell width W = 85 mm. (b) Width of downward flow developed near a side wall as a function of time, obtained from two cells with different widths, W = 55 and 125 mm, at the same f and a. (c) Superposition of snapshots in first 544 seconds for the cell with width 55 mm, visualizing the width of downward flow near the side wall. The dashed horizontal line indicates an average top surface of particles.

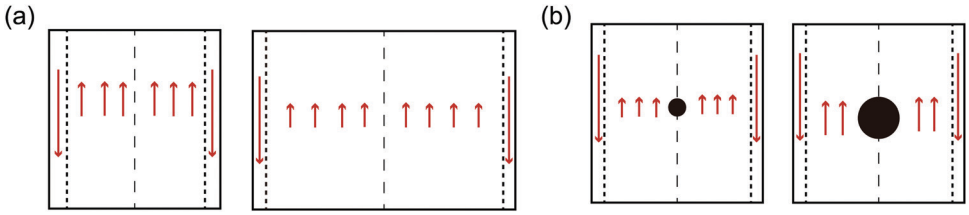

Fig. 5 (a) The effect of cell width on upward flow velocity. (b) The effect of an intruder's diameter on upward flow velocity.

disk (and away from the disk) scales with a dimensionless factor d/W as illustrated in Fig. 5a. However, alongside the disk, it scales with $d/(W-D)$ as suggested in Fig. 5b. In other words, there are two factors d/W and $d/(W-D)$, and both govern the rising velocity of the disk. Considering that the former is a decreasing function of W and the latter introduces a factor that increases with D, and expecting that the expression is independent of the smallest scale, the bead diameter d, a simplest possibility incorporating the two factors is a dimensionless factor D/W. This explains why U_2 scales with D/W in eqn (2).

This D dependence of U_2 is in contrast with results reported in previous studies:[5,10] they reported that the velocity of ascent due to convection is independent of the size of the intruder. This may because the previous cases were more insensitive to the effect; they both considered not a two-dimensional case as ours, but a three-dimensional case, and they considered cases in which the ratio of the intruder diameter to grain diameter is larger (the ratio is $\simeq$3.4–306 in ref. 5 and $\simeq$8–13 in ref. 10 while it is $\simeq$5–7 in our case).

V. Conclusion

We examined the rising motion of an intruder in an original one-layer granular bed under continuous vibration for a wide range of parameters. We found that the motion was divided into two regimes and both regimes were well characterized by vibration velocity (v) through simple scaling laws. We provided physical interpretations based on the convection and arch effects. Although the two mechanisms are closely related, they can be clearly distinguished. The arch effect explains the scaling for the first regime ($\sim v^2$), while the convection mechanism explains the second scaling ($\sim v$). These two cases emphasize the importance of vibration velocity for understanding the BN effect. This generic feature of the BN effect confirmed in the present study will be useful not only in granular physics, but also in many applications such as agriculture, and the cosmetics and pharmaceutical industries.[15,16]

Conflicts of interest

There are no conflicts to declare.

Acknowledgements

K. O. appreciates Mika Umehara (Ochanomizu University) for giving useful comments. This work was partly supported by JSPS KAKENHI Grant Number JP19H01859.

References

1 C. F. Harwood, Powder segregation due to vibration, *Powder Technol.*, 1977, **16**, 51–57.
2 J. C. Williams, The segregation of particulate materials. a review, *Powder Technol.*, 1976, **15**, 245–251.
3 A. Rosato, K. J. Strandburg, F. Prinz and R. H. Swendsen, Why the brazil nuts are on top: Size segregation of particulate matter by shaking, *Phys. Rev. Lett.*, 1987, **58**, 1038–1040.
4 E. Clément, J. Duran and J. Rajchenbach, Experimental study of heaping in a two-dimensional ''sand pile'', *Phys. Rev. Lett.*, 1992, **69**, 1189.
5 J. B. Knight, H. M. Jaeger and S. R. Nagel, Vibration-induced size separation in granular media: The convection connection, *Phys. Rev. Lett.*, 1993, **70**, 3728.
6 J. Duran, J. Rajchenbach and E. Clement, Arching effect model for particle size segregation, *Phys. Rev. Lett.*, 1993, **70**, 2431–2434.
7 R. Jullien, P. Meakin and A. Pavlovitch, Three-dimensional model for particle-size segregation by shaking, *Phys. Rev. Lett.*, 1992, **69**, 640.
8 J. B. Knight, *et al.*, Experimental study of granular convection, *Phys. Rev. E: Stat. Phys., Plasmas, Fluids, Relat. Interdiscip. Top.*, 1996, **54**, 5726.
9 L. Vanel, A. D. Rosato and R. N. Dave, Rise-time regimes of a large sphere in vibrated bulk solids, *Phys. Rev. Lett.*, 1997, **78**, 1255.
10 P. Hejmady, R. Bandyopadhyay, S. Sabhapandit and A. Dhar, Scaling behavior in the convection-driven brazil nut effect, *Phys. Rev. E: Stat., Nonlinear, Soft Matter Phys.*, 2012, **86**, 050301(R).
11 T. M. Yamada and H. Katsuragi, Scaling of convective velocity in a vertically vibrated granular bed, *Planet. Space Sci.*, 2014, **100**, 79–86.
12 M. Umehara and K. Okumura, Rising obstacle in a two-dimensional granular bed induced by continuous and discontinuous vibrations: Dynamics governed by vibration velocity, *J. Phys. Soc. Jpn.*, 2020, **89**, 035001.
13 E. Ehrichs, *et al.*, Granular convection observed by magnetic resonance imaging, *Science*, 1995, **267**, 1632–1634.
14 J. Duran, T. Mazozi, E. Clément and J. Rajchenbach, Size segregation in a two-dimensional sandpile: Convection and arching effects, *Phys. Rev. E: Stat. Phys., Plasmas, Fluids, Relat. Interdiscip. Top.*, 1994, **50**, 5138.
15 J. Duran, *Sables Poudres et Grains*, Eyrolles, Paris, 1997.
16 B. Andreotti, Y. Forterre and O. Pouliquen, *Granular media: between fluid and solid*, Cambridge University Press, 2013.